35445901_File000056_874681311.docx

Is the particle deposition in a cell exposure facility comparable to the lungs? A computer model approach

Erwin W. Karg[1], George A. Ferron[1], Stefanie Bauer[1], Sebastiano Di Bucchianico[1], Ralf Zimmermann[2]

[1] *Helmholtz Zentrum München, German Research Center for Environmental Health, Cooperation Group "Comprehensive Molecular Analytics"(CMA), Gmunder Straße 37, D-81379 Munich, Germany*

[2] *University of Rostock, Institute of Chemistry, Division of Analytical, Technical and Environmental Chemistry, Dr.-Lorenz-Weg 1, D-18051 Rostock*

Corresponding author:

E.W. Karg
C/O Helmholtz Zentrum München, German Research Center for Environmental Health, Cooperation Group CMA
P.O.Box 1129, D-85758 Neuherberg / Munich
Tel. +49 89 3187 2847
karg@helmholtz-muenchen.de

Coauthors:

george.ferron@helmholtz-muenchen.de
stefanie.bauer@helmholtz-muenchen.de
dibucchianico@helmholtz-muenchen.de
ralf.zimmermann@helmholtz-muenchen.de

Nomenclature

A	surface area of the cell layer at the ALI or in the lung
A(i)	wall area of a bronchial tube in lung generation *i*
AL	indicator for the alveolar lung region
ALI	air-liquid interface
AMTD	activity-median thermodynamic diameter
C	mass or number concentration parameter for a size distribution
CMD	count median diameter of a particle number distribution
C_p	particle number or mass in a bin of a particle sizer
D(i), L(i), N(i)	diameter, length and number of tubes in lung generation *i*
DE	deposition fraction, also "deposition"
DA	deposition per cell surface area, also "surface deposition"
D_p	diffusion constant of a particle
d_0	constant in ALI deposition model equation
d_p	particle diameter
d_{ae}	aerodynamic particle diameter
f	factor for lung volume adjustment in the HPLD model (equation 2B)
ET, TB, AL, TL	indicate extra-thoracic, tracheo-bronchial, alveolar and total lung region, respectively (Table 2)
FRC	functional respiratory capacity
GSD	geometric standard deviation of a lognormal distribution
HPLD	Hygroscopic Particle Lung Deposition model
h_t	distance of the trumpet from the cells (Figure 1B)
HW	half-width of a distribution (definition in Table 6)
i	index of a lung generation (Table 2 and Figure 2)
LV	lung volume
LVM	measured lung volume
m_0	constant in the ALI deposition model equation
MMD	mass median diameter of a particle mass distribution
Q	flow rate
r	index for the lung regions: *ET*, *TB*, *AL* and *TL*
R	radius of a tube
RH	relative humidity
R_i	radius of the inlet of the "trumpet" (Figure 1B)
RT	respiratory tract
R_w	radius of the surface area of the cell layer in a well-insert at the ALI
t	residence time
TB	indicator for the tracheo-bronchial lung region
TD	particle mass or number delivered per surface area ("tissue-delivered dose" or "dose rate", if normalized with the experiment time)
TL	indicator for the total lung
t_e	exposure duration (time)
VT	tidal volume
v_p	particle velocity
$\alpha, \beta, \gamma, \varepsilon$	constants in ALI deposition model equation
Δ	parameter for the deposition by diffusion in a tube
κ	particle shape factor

μ	parameter for the deposition by sedimentation in a tube
ρ_p	particle density
σ_g	geometric standard deviation

Introduction

Particle exposure of cell culture tissue at the air-liquid interface (ALI) is frequently used to assess toxicological endpoints and can be considered as an indicator for adverse health effects (Upadhyay and Palmberg 2018). The benefits of cell exposures at the ALI include reproducibility, physiological relevance in respiratory research and short-term or acute to mid-term exposures. Additionally, cellular parameters like genomics, proteomics and metabolomics are available for more in-depth molecular-toxicological and mechanistic studies. Thereby, the comparability of an ALI experiment with human exposure is an important question. A parameter to compare both is the mass or number of particles deposited on a cell surface area. It can be modeled by computer for both ALI and human respiratory tract (RT). The outcome is of interest for pre-experimental considerations as well as for the evaluation of experimental data. The amount of particles available for particle-cell interaction is the driving parameter behind all biological results.

The ALI exposure technique (Figure 1A and B) has been developed in the recent years (Tippe *et al.* 2002; Aufderheide and Mohr 2004; Bitterle *et al.* 2006; Mülhopt *et al.* 2008; Savi *et al.* 2008; Paur *et al.* 2011; Aufderheide *et al.* 2013). A confluent monolayer of epithelial cells on a semipermeable membrane is exposed at 37 °C and 85% relative humidity (Mülhopt *et al.* 2016). Thereby the cells are in contact with the aerosol from the apical side and with the culture medium from the basolateral side. In the stagnation point setup (Figure 1B) the flowrate (100 cm^3 min^{-1}) is too low for particle impaction. Consequently, deposition is limited to diffusion and sedimentation.

Other ALI concepts (Phillips *et al.* 2005; Savi *et al.* 2008; Bisig *et al.* 2018) choose different setups, for instance for minimum air velocity at the cell surface to mimic the situation in the alveolar space of the lungs more closely, thereby avoiding the cell stress from the radial shear flow in the stagnation point setup.

Several deposition models are available to estimate the particle deposition probability at the ALI (Comouth *et al.* 2013; Grabinski *et al.* 2015; Lucci *et al.* 2018). The model of Comouth *et al.* (2013) fits a mathematical function to data measured by electron micrograpy. It is used here, as it was verified with the ALI system similar to ours (Mülhopt *et al.* 2016; Krebs 2019). The model of Grabinski *et al.* (2015) is derived from finite element considerations together with deposition experiments and includes a mechanism for the electrically enhanced deposition of charged particles. The model of Lucci *et al.* (2018) uses pure physical parameters and therefore does not rely on mathematical functions fitted to measured data points.

Deposition in the human respiratory tract can be calculated using the ICRP model (ICRP 1994), which itself approximates experimental data on the total and regional lung deposition and the clearance in humans. The lung is functionally subdivided into the extrathoracic (*ET*), tracheo-bronchial (*TB*) and alveolar (*AL*) region. Here, regional information is available for volume, but not for wall surface area. Physical models do not have this limitation as they use a lung structure and airway deposition equations to calculate local and total particle deposition (Findeisen 1935; Landahl 1950; Beeckmans 1965; Gerrity *et al.* 1979; Yeh and Schum 1980; Ferron *et al.* 1988a; Ferron *et al.* 1988b; Hofmann and Koblinger 1990; Stapleton *et al.* 1994; Anjilvel and Asgharian 1995). The lung structure model allows the calculation of the surface area in each airway generation and the mean surface deposition in an airway.

Aerosol particle loss occurs during the transport inside an ALI device. It is modeled as the transmission in a series of tubes and bends (Karg 1993; Brockmann 2011) for the ALI. Particle inhalability is reviewed by Brown *et al.* (2013) and ICRP (1994) for the RT. Since deposition depends on particle size, density and shape, a substantial change in transmitted exposure size distribution has to be considered for aspiration to the ALI and for respiration in the lung.

The aim of this study is to compare both the deposition of aerosol particles on cells at the air-liquid interface and the deposition in the human respiratory tract. A commercially available air-liquid interface exposure station (Krebs 2019) is selected where a mathematical deposition model exists which is confirmed by experiments (Comouth *et al.* 2013). Particle deposition in the human lung is calculated with a modified version of the Hygroscopic Particle Lung Deposition (HPLD) model (Ferron *et al.* 2013). Particle deposition probability, deposition per surface area, deposition per cell and transmission are calculated for both the ALI and the RT. The results are applied to a typical emission particle size distribution.

Methods

Deposition (*DE*) is the probability for a particle to deposit on the cell layer at the ALI or in a human lung generation. Surface deposition (*DA*) is the deposition *DE* normalized by the area of the cells where the particles deposit on. The particle mass or number delivered to this surface area (also “tissue-delivered dose”, *TD*) is the particle mass or number deposited on the surface area of the cells located either at the ALI or in the regions of the respiratory tract during an experiment.

ALI deposition model

The ALI exposure system for this study is a VitroCell® "automated exposure station" (Comouth *et al.* 2013; Krebs 2019) with a central humidifier ("reactor", inlet flow rate 1 $m^3\ h^{-1}$, air conditioning to 37 °C, 85% *RH*; see Table 1B) and three exposure modules (Figure 1A). An extra module is available for clean air reference. Each module contains six wells with inserts, each of them connected individually to the humidifier by an isokinetic sampling line (graphically sketched in Figure 1A module 3). The cells in each insert are exposed via a stagnation point flow setup (Figure 1B). The particle deposition at this air-liquid interface is, according to Comouth *et al.* (2013):

$$DE_{ALI} = \alpha \left(\frac{d_p}{d_0}\right)^{\beta} + \frac{2\left(\gamma\, e^{\rho_p \varepsilon} + m_0\right)^2 d_p^2}{R_i^2} \qquad [1A]$$

where d_p is the particle diameter, ρ_p, the density, R_i the radius of the well inlet and d_0, m_0, α, β, γ and ε are constants (Table 1A). We adjusted m_0 in Table 1A by ourselves to match both graphs and measured data presented in Comouth *et al.* (2013) in their Fig. 9. Equation [1A] is valid for a size range of 40 nm ≤ dp ≤ 2 µm, a density of 1 g cm^{-3} ≤ ρ_p ≤ 2 g cm^{-3}, an airflow of 100 $cm^3\ min^{-1}$, a temperature of 37°C and a *RH* of 85% (Table 1B).

Figure 1A

The surface area at the ALI is assumed to be equal to the surface area of the membrane in an insert and to the surface area of a confluent monolayer of cells in an insert (Figure 1B):

$$A_{ALI} = \pi\, R_w^2 \qquad [1B]$$

with R_w being the radius of the insert membrane.

Figure 1B
Table 1

Lung deposition model

We use a modified version of the HPLD model (Ferron *et al.* 1988b; Ferron *et al.* 1993; Ferron *et al.* 2013). It is equipped with the structure model "Typical Path Lung Model: Human - Whole Lung" of Yeh and Schum (1980). The structure model is a set of hierarchically arranged tubes, where each tube branches into two smaller daughter-tubes with identical length and diameter, and with a defined angle between each other and with gravity (Figure 2A). All tubes with identical properties belong to the same lung generation number *i*. The structure is extended with a mouth or nose and an oropharynx (Ferron *et al.* 2013) with generation number $i = 1$ and $i = 2$, respectively. The trachea is for $i = 3$, the bronchi are for $i = 4$ to 9, the bronchioli for $i = 10$ to 19 and the alveolar ducts for $i = 20$ to 26 (Table 2; Figure 2A).

Figure 2A
Table 2

The lung structure model has been measured for a lung volume (LVM) of 5563.88 cm³ (Yeh and Schum 1980). We use a more realistic lung volume (LV) based on a functional respiratory capacity (*FRC*) of 3300 cm³ (ICRP 1994) with a correction for the tidal volume (*VT*):

$$LV = FRC + {}^{VT}/_{2} \qquad [2A]$$

Equation [2B] is used to correct the length and diameter of the lung generations from $i = 3$ to 26 by a factor of *f*:

$$f = \left(\frac{LV}{LVM}\right)^{1/3} \qquad [2B]$$

Deposition by sedimentation and diffusion in lung generation *i* is calculated for a stable laminar flow with equations from Thomas (1958) and Gormley and Kennedy (1949), deposition by impaction with an equation from Zhang *et al.* (1997), and deposition in nose and mouth with the equations from Cheng (2003). We further use the assumption made by Gerrity *et al.* (1979), that the deposition in an alveolar duct with alveoli is well described by the diameter of the alveoli.

The HPLD model is written in C-code and runs on Linux/Unix operating systems. It was updated for this study. A browser-based version is available online (Karg and Ferron 2012).

Deposition in the extrathoracic ($DE_{lung}(ET)$), tracheobronchial ($DE_{lung}(TB)$) and alveolar ($DE_{lung}(AL)$) lung region *r* as well as in the total lungs ($DE_{lung}(TL)$) is:

$$DE_{lung}(ET) = DE(1) + DE(2) \qquad [3A]$$

$$DE_{lung}(TB) = \sum_{i=3}^{19} DE(i) \qquad [3B]$$

$$DE_{lung}(AL) = \sum_{i=20}^{26} DE(i) \qquad [3C]$$

$$DE_{lung}(TL) = \sum_{r=ET,TB,AL} DE_{lung}(r) = \sum_{i=1}^{26} DE(i) \qquad [3D]$$

We assume that aerosol particles are wall-adhesive after deposition, in contrast to gas molecules.

All calculations reflect a seated male adult (ICRP 1994) breathing calmly through the mouth or the nose with a tidal volume of 750 cm^3, a respiratory frequency of 12 min^{-1}, a constant airflow of 250 $cm^3\ s^{-1}$, and an equal duration of 2.5 s for each in- and exhalation (Table 3).

Table 3

The tubular wall surface area *A(i)* of a lung generation *i* is calculated by:

$$A_{lung}(i) = \pi \; L(i)\, D(i)\, N(i) \qquad [4A]$$

where *L(i)* is the length, *D(i)* the diameter and *N(i)* the number of tubes in lung generation *i*. Mouth and nose are modeled as a box in generation 1 characterized by length *L(i=1)* and two diameters $D_1(i=1)$ and $D_2(i=1)$. Their wall surface is:

$$A(1) = 2\, L(1)\, [D_1(1) + D_2(1)] \qquad [4B]$$

The extrathoracic and bronchial surface area $A_{lung}(ET)$ and $A_{lung}(TB)$, respectively, are the sum of the duct wall area of the lung structure (Figure 2B). $A_{lung}(TL)$ is taken from literature (ICRP 1975). The alveolar wall area $A_{lung}(AL)$ is calculated from total and regional lung surface area:

$$A_{lung}(AL) = A_{lung}(TL) - A_{lung}(ET) - A_{lung}(TB) \qquad [4C]$$

Deposition per surface area

The surface deposition (*DA*) is defined as the mean deposition per surface area at the ALI or in a lung generation *i* (Table 2; Figure 2B):

$$DA_{ALI}(d_p,\rho_p) = \frac{DE_{ALI}(d_p,\rho_p)}{A_{ALI}} \qquad [5A]$$

$$DA_{lung}(r,d_p,\rho_p) = \frac{DE_{lung}(r,d_p,\rho_p)}{A_{lung}(r)} \qquad [5B]$$

Particle transmission efficiency

The deposition model for the ALI does not account for the transport loss from the ambient air outside to the cells at an insert inside (Figure 1A). A typical

transmission function for the ALI is the product of a series of transport efficiencies for flow rates in vertical tubes, horizontal tubes and bends (Karg 1993; Brockmann 2011), ranging from the ALI inlet to one of the well trumpets in the middle of the system (sections in Figure 1A to module 2; Table 1C). All sampling lines are identical as depicted in Figure 1A module 3.

For human inhalation, the inhalability function follows the ICRP (1994) convention for particle inhalation from calm air (Brown *et al.* 2013). The transport loss inside the lung depends on particle size, and it changes the transmitted size distribution during in- and exhalation. It is estimated from the HPLD model for mouth and nose breathing.

Particles deposited on the surface area

The particle number or mass deposited per surface area (*TD*) is the convolution of both size distribution and surface deposition. It is calculated for monodisperse particles by:

$$TD = Q\ t_e\ C_p\ DA, \qquad [6A]$$

for polydisperse particles at the air-liquid interface by:

$$TD_{ALI}(d_p,\rho_p) = Q\ t_e \sum_{d_p} C_p(d_p,\rho_p)\ DA_{ALI}(d_p,\rho_p) \qquad [6B]$$

and for the respiratory tract by:

$$TD_{lung}(r,d_p,\rho_p) = Q\ t_e \sum_{r}\sum_{d_p} C_p(d_p,\rho_p)\ DA_{lung}(r,d_p,\rho_p) \qquad [6C]$$

where $C_p(d_p,\rho_p)$ is the concentration in a particle sizer bin, t_e is the exposure duration and Q is either the flow rate through the ALI well (Table 1B) or the breathing minute

volume (Table 3). Note that C_p does not distinguish between number, length, surface, volume or mass and allows calculating *TD* for all the respective moments. Note also, that the expression "dose rate" commonly refers to the ratio TD/t_e, e. g. to the deposited mass per hour.

Cell size and properties

Data for cell-count and -size are given in Table 4. Three of the most commonly used cell lines in ALI studies are A549, BEAS-2B and 16HBE, which are derived from from alveolar, bronchial and human-bronchial-epithelial cells, respectively (ATCC 2018a; b; Merck 2019). All these cell lines retain many features of type-II pneumocyte cells, e.g. size or secretion of alveolar lining fluid. Type-I and type-II pneumocytes are cells of the alveolar epithelium, covering 94% and 6% of the alveolar space, respectively (Stone *et al.* 1992; ICRP 1994). We assume that the cells of the *ET* and *TB* region are similar in size to type-II pneumocytes, which themselves are close in size to A549 and in between both BEAS-2B and 16HBE (Table 4). In contrast, the surface area of type-I pneumocytes is 27-fold larger than the one of type-II pneumocytes.

Table 4

Particle size distribution for an exposure scenario

To demonstrate *TD* calculation, a lognormal particle size distribution is used which mimics an emission aerosol measurement. We approximate a diesel emission aerosol with a count median diameter (*CMD*) of 100 nm and a mean geometric standard deviation (*GSD*) of 1.6, which is typical for an emission aerosol (Table 5). Particles are spheres of unit density and not aggregated soot particles. The mass median diameter is calculated from count median diameter by the Hatch-Choate equations (Hatch and Choate 1929; Hinds 1999).

Table 5

Results

Deposition in the lung

The figures 2A and 2B show data from the lung structure model of Yeh and Schum (1980) for a mean lung volume of 3675 cm³ (equation [2A]; Table 3). Figure 2A presents the structural parameters number, length, diameter and angle for a lung generation *i*. Figure 2B presents the calculated parameters such as tube wall surface area, volume, average flow velocity and residence time.

In Figure 2C and Figure 2D the deposition is calculated as a function of both particle size and lung generation, for particles with a density of 1 g cm^{-3}, for the respiration conditions in Table 3, and for mouth and nose breathing, respectively. Compared to mouth breathing, both nano- and micron-sized particles deposit almost quantitatively in the nose.

Figure 2C, Figure 2D side by side

Comparison of ALI and lung deposition

Figure 3A shows the deposition for the ALI and for the RT regions, i. e. the output from equation [1A] and from the HPLD model. The deposition on the cells in the ALI is significantly lower than the deposition in most lung regions. Also the slopes differ significantly. The minimum of deposition is at 240 nm for the ALI and between 320 nm and 600 nm for the RT regions.

To compare ALI and lung deposition, Figure 3B shows the ratio $DE_{lung}(r)$ / DE_{ALI}, i. e. the difference between regional lung deposition and ALI deposition. At the deposition minimum $DE_{lung}(r)$ is up to 200 fold higher than DE_{ALI}. The differences can

be explained mainly by the differences in geometry between ALI and lung airways: The distance for a particle to hit a wall is considerably shorter in most lung generations than at the ALI (Figure 2A, Table 1B, Table 3). For the *ET* region, the ratio is close to 1 as the airways are wide.

Around the deposition minimum the ratio $DE_{lung}(r) / DE_{ALI}$ is relatively constant. We define the half-width (*HW*) as the diameter range with the ratio between 50% and 100% of the maximum. The *HW* for the lung regions and *TL* is listed in Table 6. A mean range is found between 40 nm and 450 nm.

Figure 3A, Figure 3B side by side
Table 6

Deposition per surface area

Figure 4A shows the surface deposition *DA* at the cell layer of the ALI and in the human respiratory tract. *DA* is considerably higher for the ALI than for any lung region because the cell area at the ALI is 4.7 cm^2 and the smallest surface area in a lung region is 90 cm^2 (Table 2).

The ratio $DA_{lung}(r) / DA_{ALI}$ in Figure 4B shows the difference between ALI and lung. All ratios are <<1 with $DA_{lung}(AL)$ being more than three orders of magnitude smaller than DA_{ALI} (Table 6).

The half-width size range of $DA_{lung}(r) / DA_{ALI}$ for the RT regions (Figure 4B) is identical with the half-width size range of the deposition ratio $DE_{lung}(r) / DE_{ALI}$ (compare with Figure 3B) as the normalizing surface area is constant for each region.

Figure 4A, Figure 4B side by side

Particle transmission efficiency

Figure 5 displays the transport efficiency for particles from calm ambient air to an ALI cell layer (aspiration) and to the human lungs for both mouth and nose

(respiration). The ALI aspiration efficiency is higher than 0.5 for the particle size range between 1 nm and 7 µm (Table 7). The inhalability for the human respiratory tract is higher than 0.5 for the particle size range from 1 nm to 50 µm (ICRP, 1994). Based on calculations with the HPLD model the transmission of aerosol particles is determined after passing the *ET* and *TB* region for both mouth and nose breathing. More than 50% of the particles in the size range from 1.6 nm to 12 µm pass the *ET* region during mouth breathing. More than 50% of the particles in the size range from 9 nm to 7 µm pass the *TB* region (Table 7). The corresponding values for nose breathing are 2 nm to 4 µm and 11 nm to 3 µm, respectively.

Figure 5
Table 7

Particles delivered to the cells

In Figure 4A additional ordinates are added on the right side showing the results for the size-resolved *TD* calculation. They follow equation [6A] for monodisperse particles. The first ordinate represents TD_{ALI} calculated for an exposure number concentration of 1 cm^{-3} or a mass concentration of 1 µg m^{-3}, an exposure time of 1 hour, and the ALI flow rate of 100 cm^3 min^{-1}. The second ordinate represents TD_{lung} calculated for the same number and mass concentration, an exposure time of 1 hour, and the breathing conditions in Table 3.

Figure 6A displays the *TD* model results for the polydisperse diesel-like emission mass distribution (Table 5). Calculations are performed with the equations [6B] and [6C]. Results show the *TD* deposited per hour per surface area. *DA* is mainly responsible for the difference between the ALI and the lung regions. Deposition is comparable within one order of magnitude for ALI, *ET* and *TB* region, but is smaller by more than one order of magnitude for the *AL* region and the total lung.

Figure 6B shows the particle number deposited on a single cell. ALI and *AL* region are better comparable here, as the human type-I pneumocytes are 27-fold larger than the other cells (see Table 4).

Figure 6A, Figure 6B side by side

Discussion

ALI deposition model

The right part of equation [1A] consists of two terms. The first term specifies diffusional deposition and depends on particle size but not on density. The second term describes sedimentation and depends on both particle size and density. Equation [1A] applies solely to the conditions in Table 1B. For highly aggregated particles ($\rho_p << 1$ g/cm³) virtually no sedimentation is expected and the second term should be constant or approach zero. According to equation [1A], however, it yields a rising deposition for a rising d_p, which is unrealistic. Additionally, one expects the sedimentation to depend on the square of the aerodynamic diameter.

Equation [1A] does not include a variable for the flow rate. Therefore we point out some aspects how the deposition depends on the airflow. The flow in the ALI is highly laminar (Re < 25). So one can expect that the typical parameters for diffusion and sedimentation of aerosol of particles from a stable laminar flow are valid . These parameters include residence time or air flow. As the flow in the ALI is highly laminar the typical parameters in the deposition equations for diffusion (Gormley and Kennedy 1949) from a laminar flow in a horizontal tube and sedimentation (Thomas 1958; Pich 1972), Δ and μ, respectively, are expected:

$$\Delta = \frac{D_p\, t}{4\, R^2} \sim \frac{1}{d_p\, Q} \qquad [7A]$$

$$\mu = v_p \frac{t}{R} \sim d_{ae}^2 \frac{t}{R} \sim \frac{d_{ae}^2}{R\,Q} \qquad [7B]$$

where v_p is the velocity of a particle by gravity, t is the residence time, d_{ae} is the aerodynamic particle diameter, R is the radius of the tube and D_p is the diffusion constant of the particle.

Additionally, we state a problem with the constants given in Comouth's Table 1 for the second term of equation [1A]. We could not reproduce the deposition in Comouth *et al.* (2013), their Figure 9, with the parameter m_0 given in their Table 1. We replaced their value for our calculations with the one given in Table 1A to get the correct approximation.

Lung deposition model

The HPLD model (see Ferron *et al.* (1988b), their Figure 7) is based on a model published by Lee *et al.* (1979) and Gerrity *et al.* (1979). It has been compared with experimental data (Heyder *et al.* 1986) for the tracheo-bronchial and alveolar lung deposition, three different respiratory conditions, tidal volumes of 500, 1000 and 1500 cm^3 and equal in- and exhalation times of 2, 4 and 2 s, respectively. The differences were less than 7% of the inhaled particle concentration in the particle size range from 100 nm to 10 µm.

The ICRP (1994) model (their Figures 12 to 15) studies the influence of age, gender and respiration conditions (their Annexe D), and reviews lung parameters of different ethnic groups (their Table 9). Differences less than 10% are found for adult female, adult male, girl and boy of an age of 15 years. Differences up to a factor of three are found between younger children and adults. It reviews the literature on spontaneous breathing showing changes in *TL* by 20% of the inhaled concentration. More recently

Molgat-Seon *et al.* (2018) published a study on additional lung parameters of specialized population groups.

We studied the degree of consistency between the data calculated with the ICRP model and our deposition model. Data for the ICRP model Annex F (1994) are for a male adult and different respiration conditions as a function of the activity median thermodynamic diameter (*AMTD*). This diameter can be set equal to the particle diameter d_p assuming a homogeneous distribution of the activity in the particle. Further the particles have a density of 3 g cm^{-3} and a shape factor of 1.5. Considering the aerodynamic diameter of such a particle, it can be approximated by a spherical particle with a density of 2 g cm^{-3} (Schmid *et al.* 2007). We restrict our consistency check to a particle size of 130 nm, which is in between the size range of 40 nm to 450 nm (Figure 3B and 4B). The nearest value in Annexe F is a particle with an *AMTD* of 100 nm. A summary of deposition values for this diameter is listed in Table 8 together with the corresponding HPLD data for a breathing rate of 0.54 m^3 h^{-1} and a *GSD* of 1.5. Differences in the output of both models for the deposition in *TB*, *AL* and *TL* are less than 20%.

A summary of deposition values for this diameter is listed in Table 8 together with the corresponding HPLD data for a breathing rate of 0.54 m^3h^{-1} and a GSD of 1.5. Differences in the output of both models for the deposition in *TB*, *AL* and *TL* are less than 12%. The corresponding differences for the other respiration conditions are 0.040 to 0.082, 0.20 to 0.21 and 0.28 to 0.35 less than a factor of 2.1.

For our calculations we use the lung structure model of Yeh and Schum (1980) as other models do (Anjilvel and Asgharian 1995; Winkler-Heil *et al.* 2014). Yu and Diu (1982) calculated the deposition for four different lung structure models including the structure used here and found a variation less than 10% of the inhaled particle

concentration; an exception was the lung structure of Weibel (1963), where the difference was up to 20%.

Table 8

Comparison of ALI and lung deposition

Figure 3A shows large differences between the ALI and the lung regions for deposition values and slopes of the curves. The values for the ratio $DE_{lung}(r) / DE_{ALI}$ differ for the *AL* region by a factor of 135 at the peaks (Figure 3B; Table 6). Near the peaks the ratio is relatively constant and a half-width range (*HW*) is defined where the ratio is between 50% and 100% of the maximum. Outside this range the ratio drops rapidly to one and below (Figure 3B). *HW* marks the particle size range, where ALI and lung *TD* can be compared reliably.

The ratio $DA_{lung}(r) / DA_{ALI}$ in Figure 4B estimates the difference between the deposited dose *TD* in the lung region *r* and the ALI. The surface deposition for the *ET*, *TB* and *AL* region is more than a factor of 10, 17 and 1180 lower than at the ALI, respectively. The factors vary only 2-fold within the *HW* range from 40 nm to 450 nm (Table 6). They are valid for quiet respiration conditions compared with the VitroCell ALI system.

For the biological (toxicological) dose, clearance processes in the *TB* and *AL* region have to be considered additionally, and also the difference in sensitivity between the ALI cell lines and the cells in the human lung regions.

Particle transmission efficiency

The ALI transmission efficiency (Figure 5) is a first guess by standard equations for particle transmission in tubes and varies noteworthy with tube length, diameter, curvature, angle with gravity and particle charge. It is calculated for a well in exposure

module 2 (Figure 1A). The 50% transmission efficiency ranges from 1 nm to 7 µm. This is much broader than the *HW* for the deposition ratio in Figures 3B and 4B. Note, however, that – according to Figure 5 – the ALI system is not capable of transferring particles larger than 7 µm to the cells. This has to be kept in mind, if – for instance – particles from mechanical grinding are used as an exposure aerosol. For standard-use, it is advisable to add a ~4 µm pre-impactor to the humidifier inlet to stabilize the aerosol distribution and to avoid excessive internal contamination.

According to Figure 5 and Table 6B the 50% transmission efficiency for aerosol particles to the lung ranges from <1 nm to >50 µm for inhalation (ICRP, 1994). For nose breathing it ranges from 2.5 nm to 3.5 µm and from 10 nm to 3.5 µm for entering the TB and AL regions, respectively. The exhaled range is 40 nm to 3 µm for both nose and mouth breathing. All particles in this size range are suitable for exposure experiments at the ALI.

Fate of particles after deposition

A major difference between ALI and the human lungs is the clearance, e. g. by ciliary activities in the lungs. A summary of the clearance of aerosol particles has been given in ICRP (1994). Particles are commonly cleared within several minutes from the trachea and within a day from the bronchioli. However uneven clearance has been reported in the upper airways and some areas are not cleared at all, e. g. near to the junction of a bifurcation (“hot spot”). Particles in the alveolar region may stay for a much longer time until they are encapsulated or phagocytized by macrophages. Additionally, particle solubility has to be considered. Lung clearance is beyond the scope of this paper. We restrict our considerations to pure particle deposition onto the geometric surface area.

Deposition of gas molecules

A particle size below 1 nm is commonly attributed to the transition zone between particles and gas- or vapor-molecules. Consequently, the deposition behavior of gas molecules has to be taken more and more into account for model calculations below 1 nm. Molecules do not adhere to the tissue any more when they touch down onto cell surface unless they are highly reactive like formaldehyde. Gases can also exert a back pressure from tissue side after some duration of exposure, with a lower deposition probability as a consequence.

Figure 2C and 2D indicate that the first generations are primarily exposed to these sub-nanometer particles. Due to high diffusivity hardly any of them reaches a lung generation $i > 10$. Only particles of the ultrafine and fine size range can penetrate further on. As a consequence, reactive gas or vapour molecules can reach the deep lung only when adsorbed on a fine particle or when there is already a backpressure from tissue side.

The ALI exposure system does not trap nano particles or gases like the *ET* and *TB* regions do. According to Figure 4B the ALI overrates reactive gas or vapor deposition by orders of magnitude compared to the lung.

A more detailed discussion of the effects of gas molecule goes beyond our scope. The model outcomes for sub-nanometer particles, however, may be useful for the design of ALI systems in future, which might also mimic the gas-to-particle relationship of semi-volatile aerosols in the RT.

Airway bifurcation

At airway bifurcations, the deposition pattern differs considerably from the average. Impaction and interception at the walls lead to uneven clearance. There are

numerous studies on flow pattern and deposition, and on the parameters governing them (Zhang *et al.* 2002; Zhang and Papadakis 2010; Zierenberg *et al.* 2013). Balásházy *et al.* (1999) modeled particle deposition for various spots in the vicinity of a bifurcation and defined enhancement factors for excess deposition. Their analysis yielded strong inhomogeneities with particle size and bifurcation geometry. They found enhancement factors up to about 100 in the upper bronchial airways. Especially for small (100 µm²) scanning elements the enhancement factors increased with decreasing spot size.

According to Figure 6A, the deposited mass at the ALI is comparable or lower than in the *TD* in the *TB* region. Therefore, electrical or phoretical particle deposition enhancement during an ALI experiment can be used to mimic the enhanced deposition of aerosol particles in the *ET* and *TB* region and at an airway bifurcation.

Factors influencing TD

The surface deposition *DA* in equation [6] explains the discrepancy between ALI and lung regions (Figure 4A and B), as it combines both deposition and surface area effects. Tippe *et al.* (2002) state the particle deposition being nearly independent of particle size (p. 215); more recent papers (Desantes *et al.* 2006; Comouth *et al.* 2013; Grabinski *et al.* 2015; Lucci *et al.* 2018) state a clear size dependency. The average deposition of more than 1% seems clearly too high; for accumulation mode particles (~200 nm) Desantes *et al.* (2006) estimate 0.65% for particles with ρ = 1.2 g cm^{-3} and Comouth *et al.* (2013) calculate 0.1% for unit density particles. In Figure 3A, a deposition probability >1% is found for particles < 30 nm and > 1.3 µm.

The exposure term $Q\ t_e$ represents the exposure air volume. It is about 90-fold larger for the lung than for the ALI system (Figure 4A; Table 1B; Table 3). It partly compensates the differences in surface deposition between ALI and lung. As the

exposure conditions are usually kept constant by the experimenters, $Q\ t_e$ is mostly a constant factor.

The size of cells influences the amount of particles being deposited on a single cell. A549 cells are frequently used as a model for the *AL* region and BEAS-2B for *TB*. Both are roughly comparable in size with each other and with the alveolar type-II pneumocytes, but are 27-fold smaller than type-I pneumocytes of the alveolar epithelium (Table 4). The different cell size of type-I pneumocytes in the lung and of A549 at the ALI makes the *TD* per single cell comparable (Figure 6B) and would – from this point of view – legitimize the ALI as a reasonable model design to mimic the cell-delivered dose in the *AL* region.

Application to particle size distribution

If only PM (particulate matter) filter samples are available, equation [6A] can be used for a quick estimation of TD_{ALI} from averaged data. The deposition per surface area *DA* is determined with respect to the predominant exposure particle size and TD_{ALI} calculated from the mass concentration C_p and $Q\ t_e$. The weighted average of the GSD range (16% to 84%) of our example distribution in Table 5 (i. e. from 62 nm to 160 nm) yields a *DE* of about 0.2%. *TD* from $PM_{2.5}$ filter samples was readily calculated to estimate an upper limit for exposure dose elsewhere (Oeder *et al.* 2014; Oeder *et al.* 2015).

For aggregated emission particles the particle concentration term C_p has to consider the effects of the aerodynamic diameter (d_p, ρ_p, shape factor and Cunningham slip correction). For diesel emissions (Kittelson *et al.* 2002; Park *et al.* 2003; Pagels *et al.* 2009) or wood combustion emissions (Leskinen *et al.* 2014), the mass-mobility relationship is to be considered. It additionally results in a considerably lower *DE*,

especially for highly aggregated particles ($\rho_p << 1$ g cm^{-3}). In this case equation [1A] is not applicable and another ALI deposition model must be applied.

For the lognormal exposure distribution (Table 5), the differences in *TD* between ALI and lung are less obvious (Figure 6A) as exposure particle concentration and particle deposition act to compensate each other: while the concentration maximum is at the deposition minimum, the rising deposition probability for nano- and micron-sized particles enhances the contribution of the exposure distribution tails.

Conclusions

- A particle size range of 40 nm to 450 nm is identified, where the ratio of both the deposition in a lung region and the deposition in the ALI varies by less than a factor of two (Figure 3B). Inside the range, the mean absolute ratio is up to 177 (Table 6). Outside the range the ratio drops down to 1 and lower. This ratio is important to compare ALI and lung deposition. The limitation of the size range is caused by the loss of particles inside the lungs before the particles reach the *TB* or *AL* region.
- The same size range is found for the ratio of the deposition per surface area in a lung region and at the ALI (Figure 4B). This factor is important to compare the particle load onto the cells. Particle load for a lung cell is more than 10-, 17- and 1180-fold lower compared to a cell at the ALI for the extrathoracic, tracheo-bronchial and alveolar lung region, respectively (Table 6). The ratio can be lower than of 10^{-5} outside the range.
- The mass delivered per surface area for the diesel emission example differs less than 10-fold between ALI, extra-thoracic and bronchial lung region. It is more than 10-fold smaller for the alveolar region and the total lung (Figure 6A). This

has to be considered when selecting cell lines for exposure experiments. For bronchial cell lines, the particle load for ALI should be slightly enhanced, e. g. electrically, as the bronchial lung dose is nearly comparable. For alveolar cell lines, a 10-fold deposition reduction should be applied to the ALI to match the particle load for both systems.

- The particles delivered to a single cell at the ALI for the diesel emission example is about the same as in the alveolar region, since the type-I pneumocytes of the alveolar epithelium are about 27-fold larger than the cells used in the air-liquid interface. The cell surface area of alveolar type-II pneumocytes and of the commonly used cell lines is roughly comparable (Figure 6B).
- The transmission efficiency for aerosol particles to both the ALI and the lung is close to one for the particle size range from 40 to 450 nm (Figure 5).
- The transmission to the lung generations becomes more limited with lung depth (Figure 5). This has to be considered in the design of ALI exposure experiments to avoid effects measured only in the ALI for particles that cannot reach the respective lung regions. This is especially the case for accompanying exposure gases.

In summary we conclude: The comparison of the aerosol particle dose between the ALI and the human lungs is possible, especially for the particle *HW* size range from 40 to 450 nm, where the ratio of ALI and lung deposition does not change more than a factor of 2. The corresponding dose correction factors for this range can be found in Table 6.

Acknowledgements. Data and ALI instrumentation was provided within the framework of the Helmholtz Virtual Institute of Complex Molecular Systems in Environmental Health (HICE). The authors wish to thank Dr. Hanns-Rudolph Paur and Sonja Mülhopt, KIT-Karlsruhe,

Germany, and Christoph Schlager, VitroCell, Waldkirch, Germany, for discussion and support.

No conflict of interest is declared by any of the authors.

References

Anjilvel, S. and B. Asgharian. 1995. A multiple-path model of particle deposition in the rat lung. *Fundamental and Applied Toxicology* 28(1):41-50.

ATCC. A549 Product specification and documentation. Last Modified 2018a. Accessed Nov 21st, 2018. http://www.lgcstandards-atcc.org/Products/All/CCL-185.aspx#documentation.

ATCC. BEAS-2B Product specification and documentation. Last Modified 2018b. Accessed Nov 21st, 2018. http://www.lgcstandards-atcc.org/Products/All/CRL-9609.aspx#documentation.

Aufderheide, M. and U. Mohr. 2004. A modified CULTEX system for the direct exposure of bacteria to inhalable substances. *Experimental and Toxicologic Pathology* 55(6):451-454.

Aufderheide, M., B. Halter, N. Mohle and D. Hochrainer. 2013. The CULTEX RFS: a comprehensive technical approach for the in vitro exposure of airway epithelial cells to the particulate matter at the air-liquid interface. *BioMed Research International* 2013:734137. doi: 10.1155/2013/734137.

Balásházy, I., W. Hofmann and T. Heistracher. 1999. Computation of local enhancement factors for the quantification of particle deposition patterns in airway bifurcations. *Journal of Aerosol Science* 30(2):185-203. doi: https://doi.org/10.1016/S0021-8502(98)00040-8.

Beeckmans, J. M. 1965. The deposition of aerosols in the respiratory tract. I. mathematical analysis and comparison with experimental data. *Canadian Journal of Physiology and Pharmacology* 43(a):157 - 172.

Bisig, C., P. Comte, M. Güdel, J. Czerwinski, A. Mayer, L. Müller, A. Petri-Fink and B. Rothen-Rutishauser. 2018. Assessment of lung cell toxicity of various gasoline engine exhausts using a versatile in vitro exposure system. *Environmental Pollution* 235:263-271. doi: 10.1016/j.envpol.2017.12.061.

Bitterle, E., E. Karg, A. Schroeppel, W. G. Kreyling, A. Tippe, G. A. Ferron, O. Schmid, J. Heyder, K. L. Maier and T. Hofer. 2006. Dose-controlled exposure of A549 epithelial cells at the air-liquid interface to airborne ultrafine carbonaceous particles. *Chemosphere* 65(10):1784-1790. doi: 10.1016/j.chemosphere.2006.04.035.

Brockmann, J. E. 2011. Aerosol Transport in Sampling Lines and Inlets. In *Aerosol Measurement*, ed. Kulkarni, P., P. A. Baron and K. Willeke, PART II TECHNIQUES, 68-105. Chichester, UK: Wiley & Sons.

Brown, J. S., T. Gordon, O. Price and B. Asgharian. 2013. Thoracic and respirable particle definitions for human health risk assessment. *Particle and Fibre Toxicology* 10:12.

Cheng, Y. S. 2003. Aerosol Deposition in the Extrathoracic Region. *Aerosol Science & Technology* 37(8):659-671. doi: DOI:10.1080/02786820300906.

Comouth, A., H. Saathoff, K. H. Naumann, S. Muelhopt, H. R. Paur and T. Leisner. 2013. Modelling and measurement of particle deposition for cell exposure at the air-liquid interface. *Journal of Aerosol Science* 63:103-114. doi: 10.1016/j.jaerosci.2013.04.009.

Desantes, J. M., X. Margot, A. Gil and E. Fuentes. 2006. Computational study on the deposition of ultrafine particles from Diesel exhaust aerosol. *Journal of Aerosol Science* 37(12):1750-1769. doi: 10.1016/j.jaerosci.2006.07.002.

Ferron, G. A., B. Haider and W. G. Kreyling. 1988a. Inhalation of salt aerosol particles — I. Estimation of the temperature and relative humidity of the air in the human upper airways. *Journal of Aerosol Science* 19(3):343-363. doi: 10.1016/0021-8502(88)90274-1.

Ferron, G. A., W. G. Kreyling and B. Haider. 1988b. Inhalation of salt aerosol particles. II. growth and deposition in the human respiratory tract. *Journal of Aerosol Science* 19(5):611-631.

Ferron, G. A., E. Karg and J. E. Peter. 1993. Estimation of deposition of polydisperse hygroscopic aerosols in the human respiratory tract. *Journal of Aerosol Science* 24(5):655-670.

Ferron, G. A., S. Upadhyay, R. Zimmermann and E. Karg. 2013. Model of the Deposition of Aerosol Particles in the Respiratory Tract of the Rat. II. Hygroscopic Particle Deposition. *Journal of Aerosol Medicine and Pulmonary Drug Delivery* 26(2):101-119. doi: 10.1089/jamp.2011.0965.

Findeisen, W. 1935. Über das Absetzen kleiner, in der Luft suspendierter Teilchen in der menschlichen Lunge bei der Atmung. *Pflügers Archiv - European Journal of Physiology* 236(1):367-379. doi: 10.1007/BF01752351.

Gerrity, T. R., P. S. Lee, F. J. Hass, A. Marinelli, P. Werner and R. V. Lourenco. 1979. Calculated deposition of inhaled particles in the airway generations of normal subjects. *Journal of Applied Physiology* 47(a):867 - 873.

Gormley, P. G. and M. Kennedy. 1949. Diffusion from a stream flowing through a cylindrical tube. *Proceedings of the Royal Irish Academy* 52(A):163 - 169.

Grabinski, C. M., S. M. Hussain and R. Mohan Sankaran. 2015. Simulations of submicron aerosol deposition at an air–liquid interface for in vitro toxicology. *Journal of Aerosol Science* 90:87-102. doi: 10.1016/j.jaerosci.2015.08.005.

Hatch, T. and S. P. Choate. 1929. Statistical description of the size properties of non uniform particulate substances. *Journal of the Franklin Institute* 207(3):369-387. doi: 10.1016/S0016-0032(29)91451-4.

Heyder, J., J. Gebhart, G. Rudolf, C. F. Schiller and W. Stahlhofen. 1986. Deposition of particles in the human respiratory tract in the size range 0.005–15 µm. *Journal of Aerosol Science* 17(5):811-825. doi: 10.1016/0021-8502(86)90035-2.

Hinds, W. C. 1999. *Aerosol Technology: Properties, Behavior, and Measurement of Airborne Particles.* 2nd ed. New York: John Wiley & Sons.

Hofmann, W. and L. Koblinger. 1990. Monte Carlo modeling of aerosol deposition in human lungs. Part II: Deposition fractions and their sensitivity to parameter variations. *Journal of Aerosol Science* 21(5):675-688.

ICRP. 1975. *Anatomical, Physiological and Metabolic Characteristics. Report of the Task Group on Reference Man. ICRP Publication 23.* Oxford, UK: Pergamon Press.

ICRP. 1994. Human respiratory tract model for radiological protection. A report of a Task Group of the ICRP. ICRP Publication 66. *Annals of the International conference on radioactive protection (ICRP)* 32(3-4):1-482.

Karg, E. 1993. Modeling of an aerosol transport system. *Journal of Aerosol Science* 24(Supplement 1):S511-S512.

Karg, E. W. and G. A. Ferron. The Hygroscopic Lung Particle Deposition Model Web Access. Last Modified 2012. Accessed Jan 23rd, 2020. https://www.helmholtz-muenchen.de/cma/forschung/topic-iii-aerosol-physik/projekte/index.html.

Kittelson, D. B., W. F. Watts and J. P. Johnson. 2002. Diesel Aerosol Sampling Methodology - CRC E-43, 1-181: University of Minnesota, Department of Mechanical Engineering, Minneapolis, MN 55455.

Krebs, T. Automated exposure systems. Last Modified 2019. Accessed March 23rd, 2019. http://www.vitrocell.com/inhalation-toxicology/exposure-systems/automated-exposure-station.

Landahl, H. D. 1950. On the removal of air-borne droplets by the human respiratory tract: II the nasal passages. *The bulletin of mathematical biophysics* 12(a):161-169.

Lee, P. S., T. R. Gerrity, F. J. Hass and R. V. Lourenco. 1979. A Model for Tracheobronchial Clearance of Inhaled Particles in Man and a Comparison with Data. *IEEE Transactions on Biomedical Engineering* BME-26(11):624-630.

Leskinen, J., M. Ihalainen, T. Torvela, M. Kortelainen, H. Lamberg, P. Tiitta, G. Jakobi, J. Grigonyte, J. Joutsensaari, O. Sippula et al. 2014. Effective density and morphology of particles emitted from small-scale combustion of various wood fuels. *Environmental Science & Technology* 48(22):13298-13306. doi: 10.1021/es502214a.

Lucci, F., N. D. Castro, A. A. Rostami, M. J. Oldham, J. Hoeng, Y. B. Pithawalla and A. K. Kuczaj. 2018. Characterization and modeling of aerosol deposition in Vitrocell® exposure systems - exposure well chamber deposition efficiency. *Journal of Aerosol Science* 123:141-160. doi: 10.1016/j.jaerosci.2018.06.015.

Merck. 16HBE14o- Human Bronchial Epithelial Cell Line. Last Modified 2019. Accessed Jul 19th, 2019. http://www.merckmillipore.com/DE/en/product/16HBE14o-Human-Bronchial-Epithelial-Cell-Line,MM_NF-SCC150.

Molgat-Seon, Y., C. M. Peters and A. W. Sheel. 2018. Sex-differences in the human respiratory system and their impact on resting pulmonary function and the integrative response to exercise. *Current Opinion in Physiology* 6:21-27. doi: 10.1016/j.cophys.2018.03.007.

Mülhopt, S., T. Krebs and H. R. Paur. 2008. Online dose determination for in vitro experiments with nano particles in the Karlsruhe exposure system. *Toxicology Letters* 180:S224-S224.

Mülhopt, S., M. Dilger, S. Diabaté, C. Schlager, T. Krebs, R. Zimmermann, J. Buters, S. Oeder, T. Wäscher, C. Weiss et al. 2016. Toxicity testing of combustion aerosols at the air–liquid interface with a self-contained and easy-to-use exposure system. *Journal of Aerosol Science* 96:38-55. doi: 10.1016/j.jaerosci.2016.02.005.

Oeder, S., O. Sippula, T. Streibel, H. Paur, S. Muelhopt, J. M. Arteaga-Salas, H. Harndorf, R. Zimmermann, C. B. Schmidt-Weber and J. T. M. Buters. 2014. Immunological effects of ship diesel emissions in on-line exposed human bronchial epithelial cells. *Allergy* 69:454.

Oeder, S., T. Kanashova, O. Sippula, S. C. Sapcariu, T. Streibel, J. M. Arteaga-Salas, J. Passig, M. Dilger, H.-R. Paur, C. Schlager et al. 2015. Particulate Matter from Both Heavy Fuel Oil and Diesel Fuel Shipping Emissions Show Strong Biological Effects on Human Lung Cells at Realistic and Comparable <italic>In Vitro</italic> Exposure Conditions. *PLoS ONE* 10(6):e0126536. doi: 10.1371/journal.pone.0126536.

Pagels, J., A. F. Khalizov, P. H. McMurry and R. Y. Zhang. 2009. Processing of Soot by Controlled Sulphuric Acid and Water Condensation: Mass and Mobility Relationship. *Aerosol Science and Technology* 43(7):629 - 640. doi: 10.1080/02786820902810685.

Park, K., F. Cao, D. B. Kittelson and P. H. McMurry. 2003. Relationship between particle mass and mobility for diesel exhaust particles. *Environmental Science & Technology* 37(3):577-583. doi: 10.1021/es025960v.

Paur, H.-R., F. R. Cassee, J. Teeguarden, H. Fissan, S. Diabate, M. Aufderheide, W. G. Kreyling, O. Hänninen, G. Kasper, M. Riediker et al. 2011. In-vitro cell exposure studies for the assessment of nanoparticle toxicity in the lung—A dialog between aerosol science and biology. *Journal of Aerosol Science* 42(10):668-692. doi: 10.1016/j.jaerosci.2011.06.005.

Phillips, J., B. Kluss, A. Richter and E. D. Massey. 2005. Exposure of Bronchial Epithelial Cells to Whole Cigarette Smoke: Assessment of Cellular Responses. *Atla-Alternatives to Laboratory Animals* 33:239-248.

Pich, J. 1972. Theory of Gravitational Deposition of Particles from Laminar Flows in Channels. *Aerosol Science* 3(351-361).

Savi, M., M. Kalberer, D. Lang, M. Ryser, M. Fierz, A. Gaschen, J. Ricka and M. Geiser. 2008. A novel exposure system for the efficient and controlled deposition of aerosol particles onto cell cultures. *Environ Sci Technol* 42(15):5667-5674. doi: 10.1021/es703075q.

Schmid, O., E. Karg, D. E. Hagen, P. D. Whitefield and G. A. Ferron. 2007. On the effective density of non-spherical particles as derived from combined measurements of aerodynamic and mobility equivalent size. *Journal of Aerosol Science* 38(4):431-443.

Stapleton, K. W., W. H. Finlay and P. Zuberbuhler. 1994. An In Vitro Method for Determining Regional Dosages Delivered by Jet Nebulizers. *Journal of Aerosol Medicine* 7(4):325-344.

Stone, K. C., R. R. Mercer, P. Gehr, B. Stockstill and J. D. Crapo. 1992. Allometric relationships of cell numbers and size in the mammalian lung. *American Journal of Respiratory Cell and Molecular Biology* 6(2):235-243.

Thomas, J. W. 1958. Gravity Settling of Particles in a Horizontal Tube. *Journal of the Air Pollution Control Association* 8(1):32-34. doi: 10.1080/00966665.1958.10467825.

Tippe, A., U. Heinzmann and C. Roth. 2002. Deposition of fine and ultrafine aerosol particles during exposure at the air/cell interface. *Journal of Aerosol Science* 33(2):207-218.

Upadhyay, S. and L. Palmberg. 2018. Air-Liquid Interface: Relevant In Vitro Models for Investigating Air Pollutant-Induced Pulmonary Toxicity. *Toxicol Sci* 164(1):21-30. doi: 10.1093/toxsci/kfy053.

Weibel, E. R. 1963. *Morphometry of the Human Lung.* Berlin: Springer Verlag.

Winkler-Heil, R., G. Ferron and W. Hofmann. 2014. Calculation of hygroscopic particle deposition in the human lung. *Inhalation Toxicology* 26(3):193-206. doi: 10.3109/08958378.2013.876468.

Yeh, H.-C. and G. M. Schum. 1980. Models of human lung airways and their application to inhaled particle deposition *Bulletin of Mathematical Biology* 42:461~480.

Yu, C. P. and C. K. Diu. 1982. A comparitive study of aerosol deposition in different lung models. *American Industrial Hygiene Association Journal* 43(a):54 - 65.

Zhang, H. and G. Papadakis. 2010. Computational analysis of flow structure and particle deposition in a single asthmatic human airway bifurcation. *Journal of Biomechanics* 43(13):2453-2459. doi: 10.1016/j.jbiomech.2010.05.031.

Zhang, L., B. Asgharian and S. Anjilvel. 1997. Inertial Deposition of Particles in the Human Upper Airway Bifurcations. *Aerosol Science and Technology* 26(2):97-110. doi: 10.1080/02786829708965417.

Zhang, Z., C. Kleinstreuer, C. S. Kim and A. J. Hickey. 2002. Aerosol transport and deposition in a triple bifurcation bronchial airway model with local tumors. *Inhalation Toxicology* 14(11):1111-1133. doi: 10.1080/08958370290084809.

Zierenberg, J. R., D. Halpern, M. Filoche, B. Sapoval and J. B. Grotberg. 2013. An asymptotic model of particle deposition at an airway bifurcation. *Mathematical Medicine and Biology* 30(2):131-156. doi: 10.1093/imammb/dqs002.

Figure Captions

Figure 1A. Scheme of a VitroCell automated exposure station (air-liquid interface exposure system). The aerosol path from outside to the exposure site is kept at a temperature of 37°C by the system containment heater and circulation. It is conditioned to a relative humidity of 85% in the humidifier. The particles are isokinetically sampled from the humidifier and transported to the exposure wells in horizontal sampling lines. Flow rate through the well is controlled for 100 cm^3 min^{-1}. Six wells are grouped into an exposure module. The system holds three modules with identical properties. One exposure module is used for clean air reference. The section numbers indicate the calculation steps for particle loss estimation (Table 1C).

Figure 1B. Scheme of the air-liquid interface (ALI) exposure setup. The aerosol is delivered to the ALI via a trumpet-shaped flow-guiding element. Particles deposit onto the cells by diffusion and sedimentation. The well keeps the insert in place. Cells grow on a membrane in the insert with the medium from the basolateral and the exposure aerosol from the apical side. R_i is the inlet radius, R_w the radius of the membrane of an insert in a well and h_t the distance of the trumpet from the cell membrane (see Table 1B)

Figure 2A. Parameters of the lung structure model of Yeh and Schum (1980) corrected for a mean lung volume of 3 675 cm^3 with equation [2B]. The model is extended with a nose or mouth and an oropharynx (Ferron *et al.* 1988a; Ferron *et al.* 1988b). Data are presented as a function of the lung generation i. Nose or mouth is $i = 1$, the oropharynx $i = 2$, the trachea $i = 3$, the main bronchi $i = 4$, the last bronchi $i = 11$, the bronchioles $i = 12$ to 19 and the alveolar ducts $i = 20$ to 26 (ICRP 1994). Background colors indicate the extra-thoracic (*ET*, green), tracheo-bronchial (*TB*, blue) and alveolar (*AL*, red) lung region.

Figure 2B. Parameters calculated from the lung structure model of Yeh and Schum (1980) (Figure 2A). Surface area $A_{lung}(i)$ of a lung generation i is calculated with equation [4].

Figure 2C. Lung deposition calculated with the HPLD model as a function of lung generation and particle size. Blue color marks nearly zero deposition, red color maximum deposition. Calculation is performed for spherical particles with a density of 1 g cm^{-3} and for a sitting male adult breathing by mouth with a tidal volume of 750 cm^3, a constant respiration airflow, an equal in- and exhalation time (Table 3).

Figure 2D. Same as Figure 2C, but for nose breathing.

Figure 3A. ALI and regional lung deposition. Deposition at the ALl is calculated with equation [1A] as a function of particle size. Total and regional lung deposition is calculated with the HPLD model for mouth respiration. Modeling conditions are listed in Table 1A and Table 3 for ALI and lung, respectively.

Figure 3B. Ratio $DE_{lung}(r) / DE_{ALI}$ of the regional lung deposition and the ALI deposition (Figure 3A. The horizontal bars show the half-width for the *ET* (green), *TB* (blue), *AL* (red) and *TL* (yellow) region (Table 6).

Figure 4A. Deposition per surface area for the ALI and for the lung regions. Mean surface deposition in the ALl is calculated with equation [5A] as a function of particle size. Total and regional lung surface deposition is calculated with the HPLD model for mouth respiration using equation [5B] (see Table 1, 2 and 3). The ordinates on the right show the corresponding particle number and mass delivered per surface area at the ALI and in the lung regions. They are calculated with equation [6B] and [6C], respectively. Ordinates represent simultaneously the *TD* for an exposure number concentration of 1 cm^{-3} and for an exposure mass concentration of 1 µg m^{-3}. Thereby t_e is set to 1 h for both ALI and lung and Q to 100 cm^3 min^{-1} (Table 1B) for the ALI and to 0.54 m^3 h^{-1} for the lung, what results in a constant factor of 6×10^3 and 540×10^3, respectively.

Figure 4B. Ratio $DA_{lung}(r) / DA_{ALI}$ of the regional lung surface deposition and the ALI surface-deposition (Figure 4A). The horizontal bars show the half-width for the *ET* (green), *TB* (blue), *AL* (red) and *TL* (yellow) region (Table 6).

Figure 5. Particle transmission to the site of deposition as a function of particle size. ALI transmission is calculated (without any pre-impactor) from the ALI inlet to a well (see Table 1C and Figure 1A). Human inhalability follows the ICRP convention (Brown et al. 2013). Mouth and nose transmission is calculated with the HPLD model, showing the particle transfer to the beginning of the tracheo bronchial tract (*TB*, $i > 2$) and to the beginning of the alveolar space (*AL*, $i > 19$). The transmission efficiency for exhaled particles is added. The expression „mouth to TB“ is used as a shortcut for “mouth breathing to enter the tracheo-bronchial region”, and „mouth to AL“ as a shortcut for “mouth breathing to enter the alveolar region”.

Figure 6. Surface-delivered particle mass (A) and cell-delivered particle number (B) at the ALI and in the lung regions. The airborne exposure concentration is 1 mg m^{-3} in (A) and 10^6 cm^{-3} in (B). A lognormal emission distribution is applied (see Table 5). Part (B) compares the load for cells in different lung regions. The corresponding cell counts (cells per cm^2) are indicated in the columns. For the ALI, the size of A549 cells is assumed, for *ET* and *TB* region the cell size is assumed to be identical with type-II pneumocytes. For the *AL* region the size of type-I pneumocytes and for *TL* the weighted average of type-I and type-II cells is assumed (Table 4).

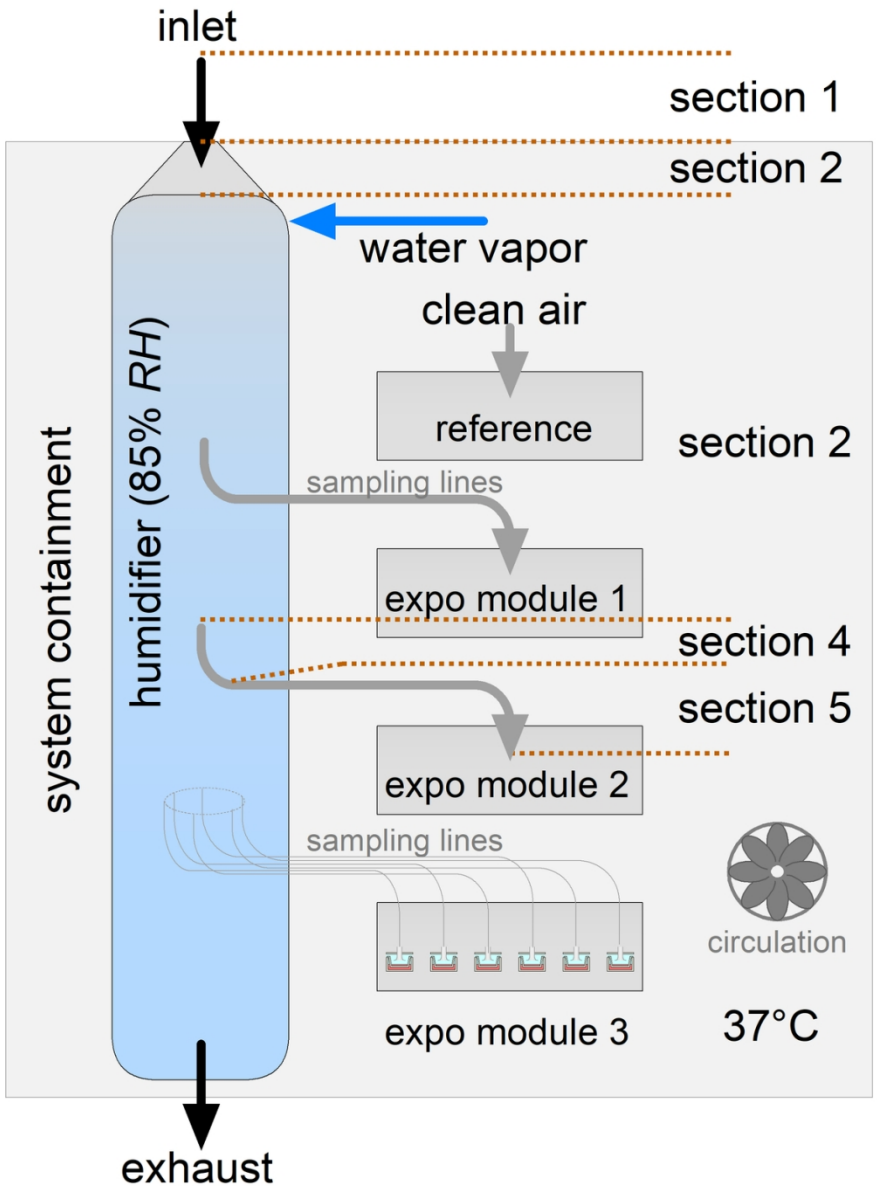

Figure 1A. Scheme of a VitroCell automated exposure station (air-liquid interface exposure system). The aerosol path from outside to the exposure site is kept at a temperature of 37°C by the system containment heater and circulation. It is conditioned to a relative humidity of 85% in the humidifier. The particles are isokinetically sampled from the humidifier and transported to the exposure wells in horizontal sampling lines. Flow rate through the well is controlled for 100 cm3 min-1. Six wells are grouped into an exposure module. The system holds three modules with identical properties. One exposure module is used for clean air reference. The section numbers indicate the calculation steps for particle loss estimation (Table 1C).

99x135mm (300 x 300 DPI)

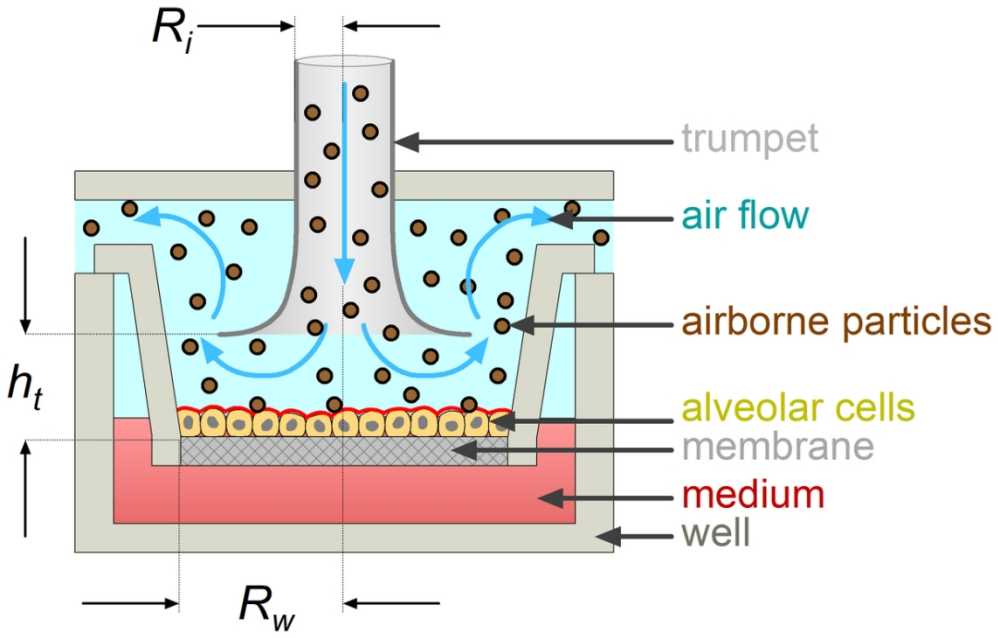

Figure 1B. Scheme of the air-liquid interface (ALI) exposure setup. The aerosol is delivered to the ALI via a trumpet-shaped flow-guiding element. Particles deposit onto the cells by diffusion and sedimentation. The well keeps the insert in place. Cells grow on a membrane in the insert with the medium from the basolateral and the exposure aerosol from the apical side. Ri is the inlet radius, Rw the radius of the membrane of an insert in a well and ht the distance of the trumpet from the cell membrane (see Table 1B)

103x67mm (300 x 300 DPI)

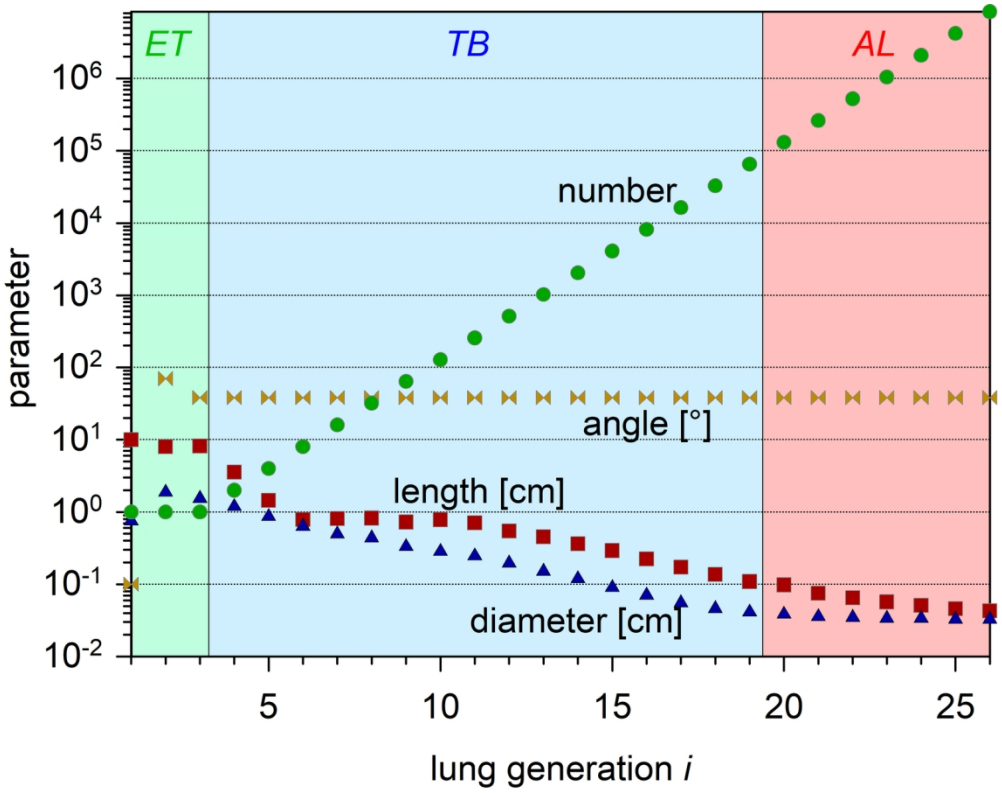

Figure 2A. Parameters of the lung structure model of Yeh and Schum (1980) corrected for a mean lung volume of 3 675 cm³ with equation [2B]. The model is extended with a nose or mouth and an oropharynx (Ferron et al. 1988a; Ferron et al. 1988b). Data are presented as a function of the lung generation i. Nose or mouth is i = 1, the oropharynx i = 2, the trachea i = 3, the main bronchi i = 4, the last bronchi i = 11, the bronchioles i = 12 to 19 and the alveolar ducts i = 20 to 26 (ICRP 1994). Background colors indicate the extra-thoracic (ET, green), tracheo-bronchial (TB, blue) and alveolar (AL, red) lung region.

139x110mm (300 x 300 DPI)

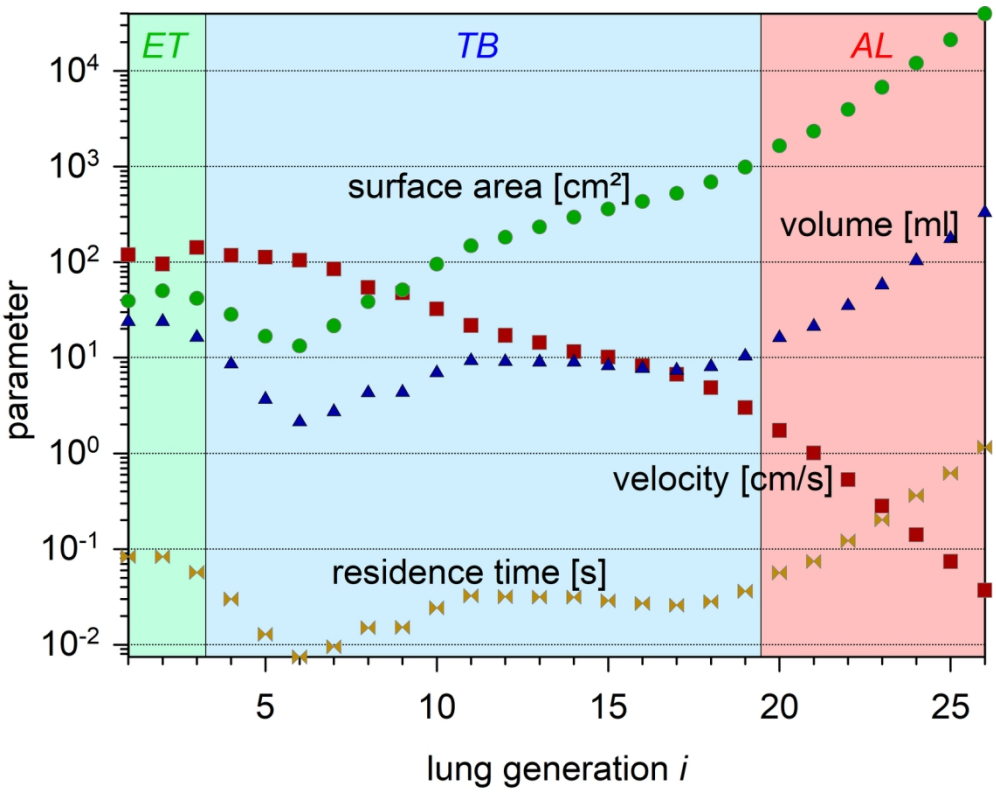

Figure 2B. Parameters calculated from the lung structure model of Yeh and Schum (1980) (Figure 2A). Surface area Alung(i) of a lung generation i is calculated with equation [4].

140x110mm (300 x 300 DPI)

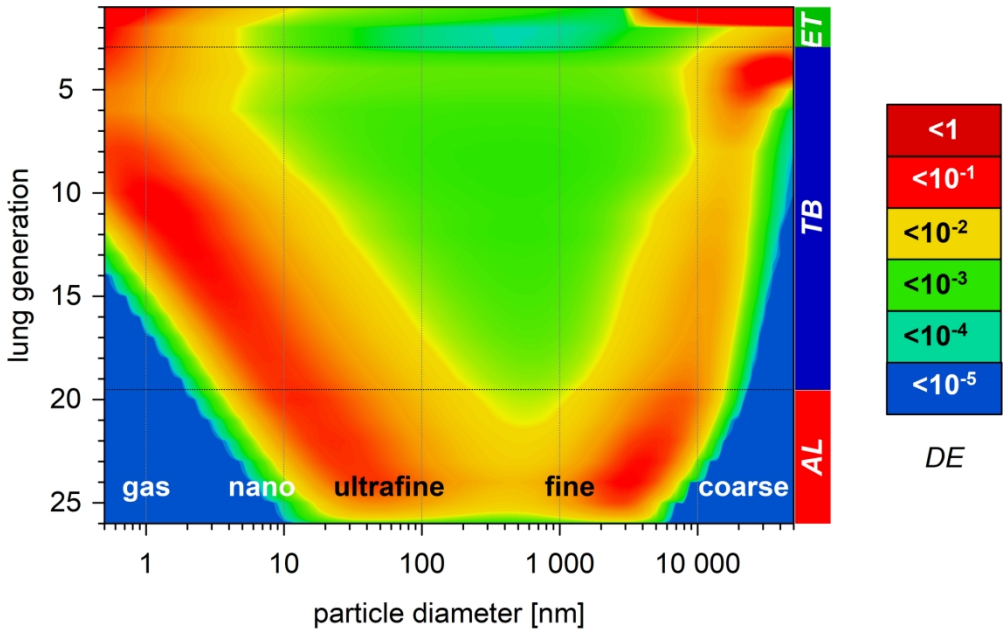

Figure 2C. Lung deposition calculated with the HPLD model as a function of lung generation and particle size. Blue color marks nearly zero deposition, red color maximum deposition. Calculation is performed for spherical particles with a density of 1 g cm 3 and for a sitting male adult breathing by mouth with a tidal volume of 750 cm³, a constant respiration airflow, an equal in- and exhalation time (Table 3).

174x109mm (300 x 300 DPI)

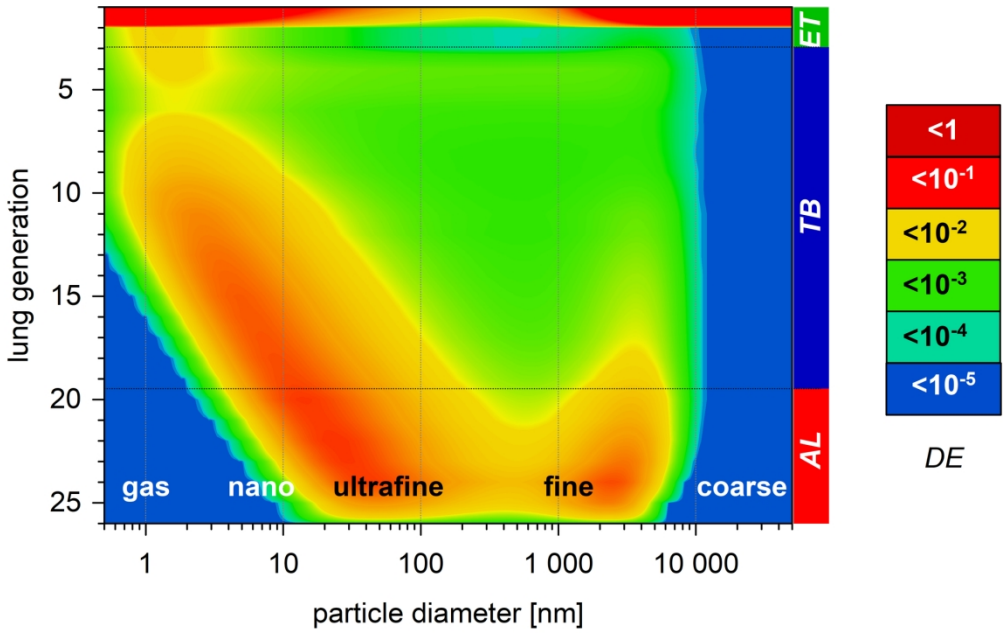

Figure 2D. Same as Figure 2C, but for nose breathing.

174x109mm (300 x 300 DPI)

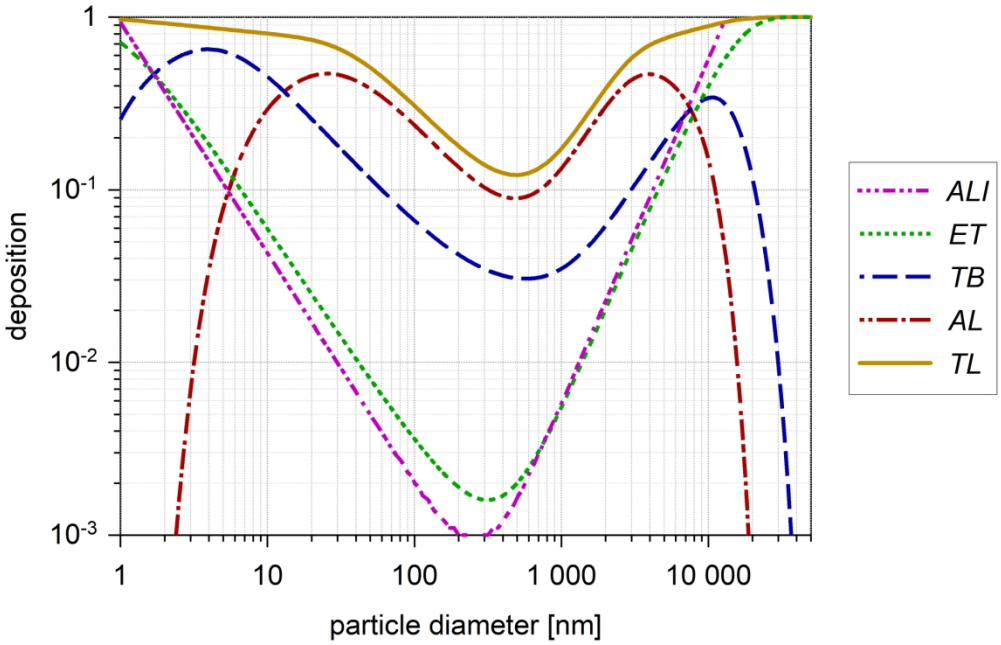

Figure 3A. ALI and regional lung deposition. Deposition at the ALI is calculated with equation [1A] as a function of particle size. Total and regional lung deposition is calculated with the HPLD model for mouth respiration. Modeling conditions are listed in Table 1A and Table 3 for ALI and lung, respectively.

173x112mm (300 x 300 DPI)

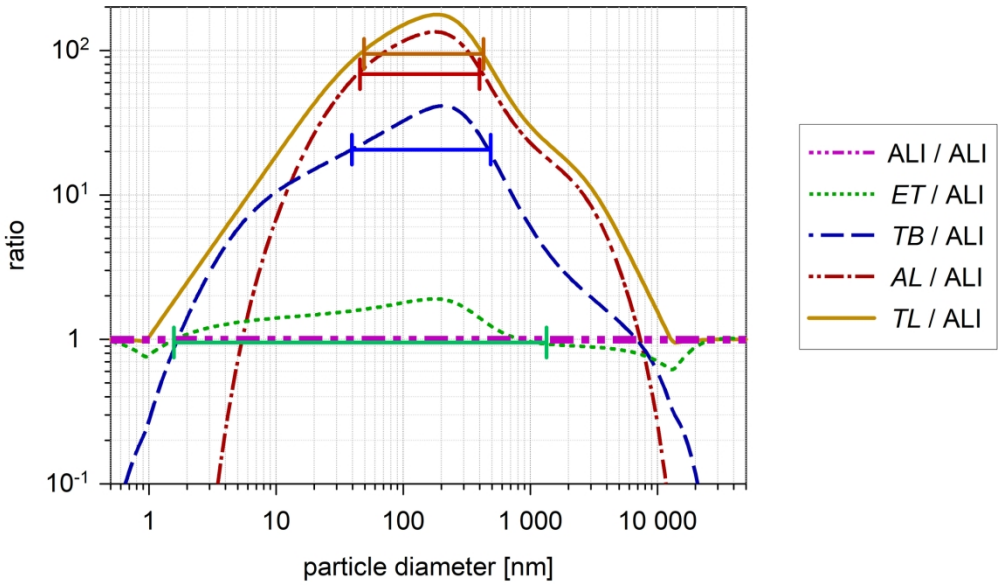

Figure 3B. Ratio DElung(r) / DEALI of the regional lung deposition and the ALI deposition (Figure 3A. The horizontal bars show the half-width for the ET (green), TB (blue), AL (red) and TL (yellow) region (Table 6).

188x109mm (300 x 300 DPI)

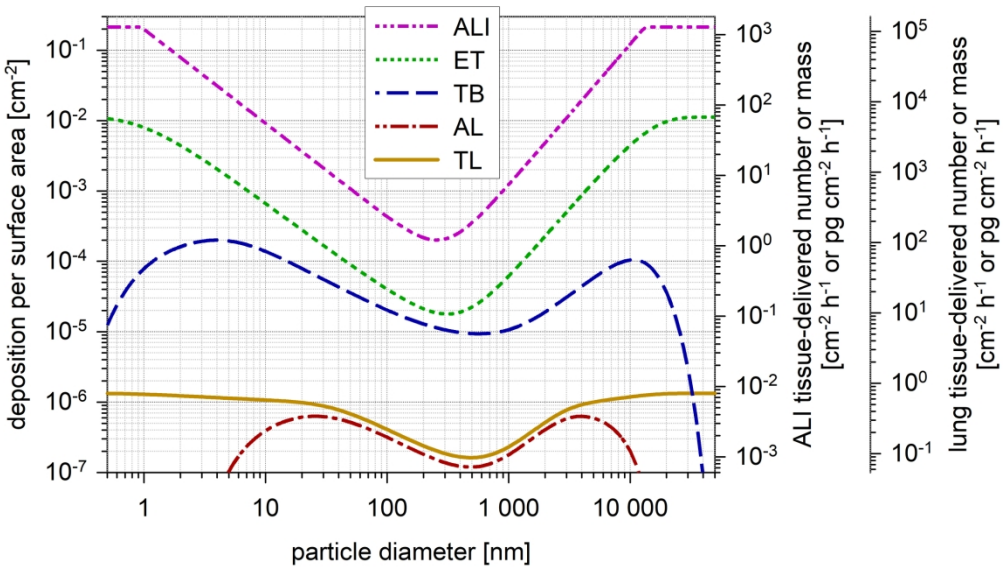

Figure 4A. Deposition per surface area for the ALI and for the lung regions. Mean surface deposition in the ALI is calculated with equation [5A] as a function of particle size. Total and regional lung surface deposition is calculated with the HPLD model for mouth respiration using equation [5B] (see Table 1, 2 and 3). The ordinates on the right show the corresponding particle number and mass delivered per surface area at the ALI and in the lung regions. They are calculated with equation [6B] and [6C], respectively. Ordinates represent simultaneously the TD for an exposure number concentration of 1 cm 3 and for an exposure mass concentration of 1 µg m 3. Thereby te is set to 1 h for both ALI and lung and Q to 100 cm3 min-1 (Table 1B) for the ALI and to 0.54 m3 h-1 for the lung, what results in a constant factor of 6 × 103 and 540 × 103, respectively.

197x111mm (300 x 300 DPI)

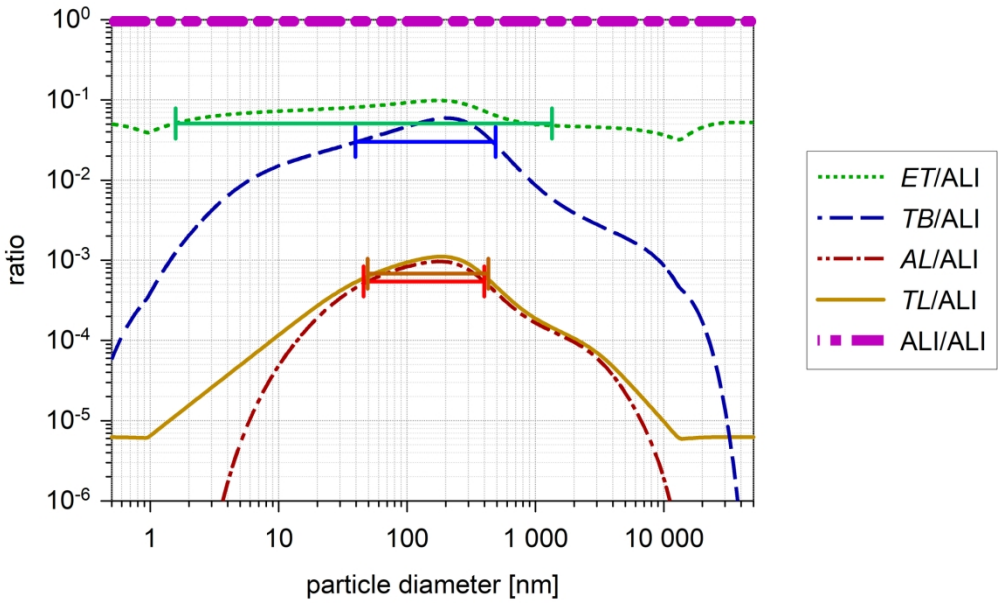

Figure 4B. Ratio DAlung(r) / DAALI of the regional lung surface deposition and the ALI surface-deposition (Figure 4A). The horizontal bars show the half-width for the ET (green), TB (blue), AL (red) and TL (yellow) region (Table 6).

186x112mm (300 x 300 DPI)

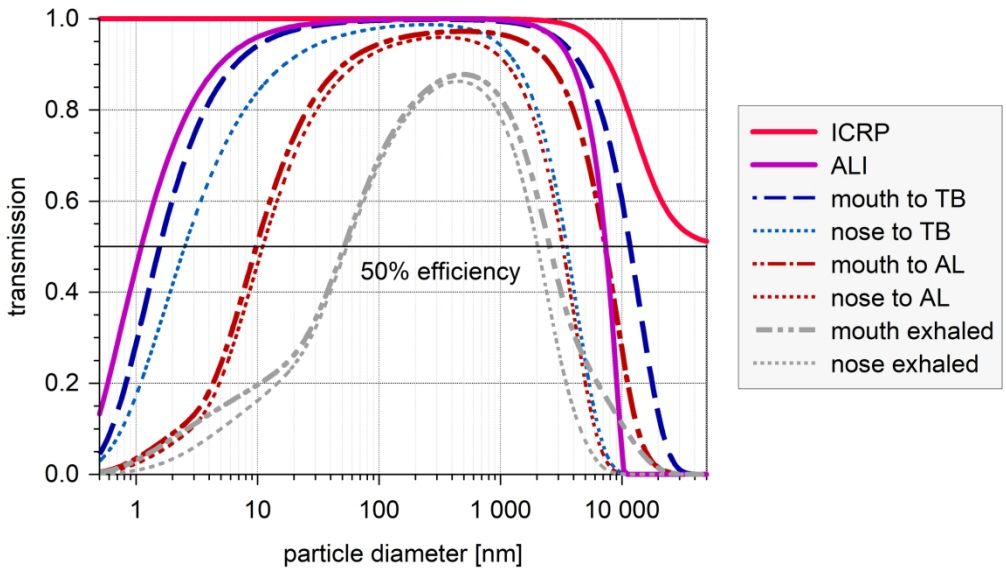

Figure 5. Particle transmission to the site of deposition as a function of particle size. ALI transmission is calculated (without any pre-impactor) from the ALI inlet to a well (see Table 1C and Figure 1A). Human inhalability follows the ICRP convention (Brown et al. 2013). Mouth and nose transmission is calculated with the HPLD model, showing the particle transfer to the beginning of the tracheo bronchial tract (TB, i > 2) and to the beginning of the alveolar space (AL, i > 19). The transmission efficiency for exhaled particles is added. The expression „mouth to TB" is used as a shortcut for "mouth breathing to enter the tracheo-bronchial region", and „mouth to AL" as a shortcut for "mouth breathing to enter the alveolar region".

197x112mm (300 x 300 DPI)

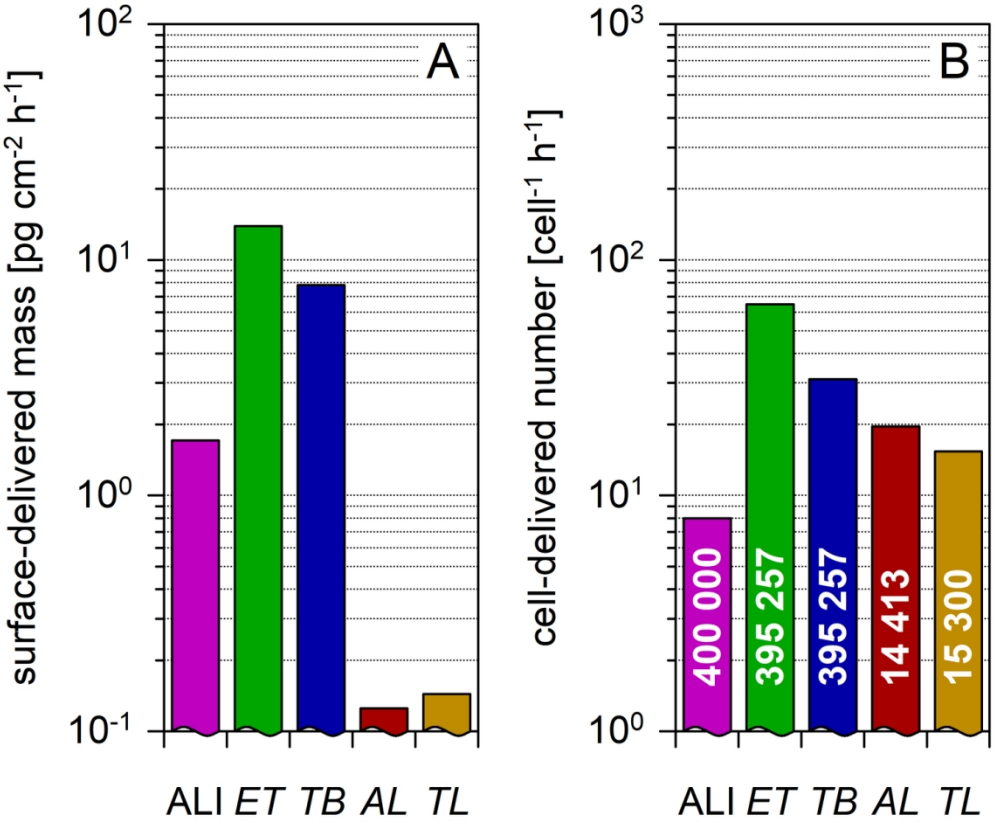

Figure 6. Surface-delivered particle mass (A) and cell-delivered particle number (B) at the ALI and in the lung regions. The airborne exposure concentration is 1 mg m-3 in (A) and 106 cm 3 in (B). A lognormal emission distribution is applied (see Table 5). Part (B) compares the load for cells in different lung regions. The corresponding cell counts (cells per cm²) are indicated in the columns. For the ALI, the size of A549 cells is assumed, for ET and TB region the cell size is assumed to be identical with type-II pneumocytes. For the AL region the size of type-I pneumocytes and for TL the weighted average of type-I and type-II cells is assumed (Table 4).

127x105mm (300 x 300 DPI)

Table 1. ALI characteristics.

Table 1A. Parameters for the ALI deposition equation [1A] are taken from Comouth et al. (2013), his Table 1. The value for m0 is modified here to fit the experimental data in his Figure 9.. Model results are valid for the operational parameters in Table 1B.

Table 1B. Operational and geometric parameters of the ALI setup.

Table 1C. Parameters for the estimation of the particle transmission from the inlet of a VitroCell automated exposure station to the inlet of a well-trumpet (see Figure 1A)

Identifier	***Value***	***Unit***	***Meaning***
		A. ALI deposition model	
α	8.81×10^{-13}	-	Constant
β	-1.33618	-	Constant
γ	-905.207	-	Constant
ε	9.71×10^{-5}	$m^3\ kg^{-1}$	Constant
d_0	1	m	Normalization constant
m_0	805.16	-	constant m_0 = 1015.43 in Comouth *et al.* (2013)
R_i	3×10^{-3}	m	Inlet radius
ρ_p	1000	$kg\ m^{-3}$	Particle density
		B. ALI Operational and geometric parameters	
Q	100	$cm^3\ min^{-1}$	Well flow rate
	37	°C	Aerosol temperature
	85	%	Aerosol relative humidity
R_w	12.2	mm	Radius a well
h_t	2	mm	Distance of trumpet from membrane surface (Comouth *et al.* 2013)
		C. ALI Particle Transmission Estimation	
Q_{asp}	1	$m^3\ h^{-1}$	ALI inlet flow rate
d_i; L	10; 250	mm; mm	Section 1: Vertical inlet tube after pre-impactor: diameter; length
D_1; D_2; L	10; 50; 50	mm; mm; mm	Section 2: Vertical transition cone to reactor: inlet diameter; outlet diameter; length
d_i; L	50; 400	mm; mm	Section 3: Vertical reactor: diameter; length
$d_{i\,i}$; L	4; 50	mm; mm	Section 4: Isokinetic sampling tube: diameter; length
Q	100	$cm^3\ min^{-1}$	Flow rate through sampling tube to well-trumpet
φ; R_φ; d_i	90; 20; 4	°; mm; mm	Bend in sampling tube: bend angle; bend radius; tube diameter
Θ; d_i; L	0; 4; 200	°; mm; mm	Section 5: Horizontal transfer line to the well, sedimentation: angle with gravity; diameter; length
$d_{i\,i}$; L	4; 200	mm; mm	Transfer line to the well, diffusion: diameter; length
φ; R_φ; d_i	90; 50; 4	°; mm; mm	Bend in transfer hose: angle of bend; radius of bend; tube diameter
d_i; L	4; 50	mm; mm	Vertical transfer hose to trumpet: diameter; length

Table 2. Surface area of the cell layer at the ALI and of the lung structure of Yeh and Schum (1980) corrected for a lung volume of 3675 cm³. The alveolar surface area is calculated with equation [4C]. Total lung surface area is taken from Reference Man (ICRP 1975).

Region	***Surface Area***		***Lung Generation***	***Meaning***
r	***A(r)***	***unit***	***i***	
ALI	4.7	cm²	-	Cell area air-liquid interface
ET	89.5	cm²	1, 2	Mouth and nose, extrathoracic region
TB	0.33	m²	3-19	Tracheo-bronchial region
AL	74.7	m²	20-26	Alveolar region
TL	75	m²	-	Total lung (ICRP 1975)

Table 3. Parameters used for the HPLD model calculations (Ferron et al. 2013). The respiration conditions are for a quiet breathing male person (ICRP 1994).

Parameter	***Value***	***Unit***
Particle density (non-hygroscopic)	1.0	g/cm³
Breathing path	mouth and nose	-
Inhalation / exhalation time	2.5 / 2.5	s
Breath duration	5	s
Breathing frequency	12	min^{-1}
Breathing minute volume	9×10^3	$cm^3\ min^{-1}$
Hourly breath flow rate	0.54	$m^3\ h^{-1}$
In- and exhalation airflow	250	$cm^3\ s^{-1}$
Functional Residual Capacity (*FRC*)	3300	cm³
Lung volume (*LV*)	3675	cm³
Tidal Volume (*VT*)	750	cm³
Mouth & oropharynx	50	cm³
Nose & nasopharynx	50	cm³

Table 4. Properties of several human lung cells and ALI cell lines. The weighted average of type-I and type-II pneumocytes is used for the *TL* calculations, as type-I cells contribute 94% to the epithelial surface area and type-II cells 6% . For the ALI exposure, the A549 cell line is assumed. BEAS-2B and 16HBE cell lines are included for comparison.

Cell Species	***Number of Cells per Surface Area [cells per cm²]***	***Area of one Cell [µm²]***	***Remarks***
Human type-I pneumocytes [a]	14 413	6 938	Human alveolar lung cell
Human type-II pneumocytes [a]	395 257	253	Human alveolar lung cell
Weighted average type-I and type-II [a]	15 300	6 536	Average of total lung
A549 [c]	400 000	250	Alveolar cell line
BEAS-2B [b]	300 000	333	Bronchial cell line
16HBE140 [b]	700 000	143	Human bronchial epithelial cell line

[a](Stone *et al.* 1992); [b](ATCC 2018; 2019); [c](Lenz *et al.* 2009)

Table 5. Parameters for the lognormal particle size distribution used as airborne particle exposure scenario. It mimics the size distribution of a diesel emission with 100 nm modal diameter. The corresponding mass median diameter is derived by Hatch-Choate conversion (Hinds 1999). Number and mass distribution are adjusted for a total concentration of 10^6 cm^{-3} and 1 mg m^{-3}, respectively.

Particle Emission Distribution Scenario				
Parameter	***Number***	***Mass***	***Unit***	***Meaning***
median	100	194	nm	Count or mass median diameter
σ_g	1.6	1.6	-	Geometric standard deviation
C	10^6	7.07×10^5	cm^{-3}	Number concentration parameter
Total sum	10^6 cm^{-3}	1 mg m^{-3}		Total concentration

Table 6. Half-width ranges for the ratio $DE_{lung}(r) / DE_{ALI}$ and $DA_{lung}(r) / DA_{ALI}$. All values between the maximum (100%) and half of the maximum (50%) of a size distribution are found within the HW range (Figure 3B and 4B). The value "mean" is at ¾ of the maximum. $Ratio^{-1}$ is the inverse DA-ratio meaning how many fold the dose at the ALI is higher than in the lung.

Region	***Half-Width Range [nm]***		***Ratio $DE_{lung}(r)/DE_{ALI}$*** (Figure 3B)			***Ratio $DA_{lung}(r)/DA_{ALI}$*** (Figure 4B)			***$Ratio^{-1}$***	
r	***lower***	***upper***	***100%***	***mean***	***50%***	***100%***	***mean***	***50%***	***100%***	***mean***
ET	1.47	1075	1.88	1.41	0.938	9.85×10^{-2}	7.39×10^{-2}	4.93×10^{-2}	10.2	13.5
TB	39.8	468	41.4	31.1	20.7	5.89×10^{-2}	4.42×10^{-2}	2.95×10^{-2}	17.0	22.6
AL	42.8	429	135	101	67.3	8.47×10^{-4}	6.35×10^{-4}	4.23×10^{-4}	1180	1575
TL	41.8	438	177	133	88.6	1.11×10^{-3}	8.33×10^{-4}	5.55×10^{-4}	901	1201

Table 7. Particle size range for 50% transmission efficiency to the ALI and to different lung regions (Figure 5). The 50% transmission efficiency of the exhaled particles is indicated for comparison.

Particle Size Ranges for 50% Transmission Efficiency				
Region	***Range***			
r	***lower***		***upper***	
ALI	1.10	nm	7.37	µm
ICRP	-	nm	>50	µm
mouth to *TB*	1.56	nm	11.7	µm
nose to *TB*	2.47	nm	3.56	µm
mouth to *AL*	9.44	nm	7.44	µm
nose to *AL*	10.5	nm	3.36	µm
mouth exhaled	42.7	nm	2.89	µm
nose exhaled	44.0	nm	2.28	µm

Table 8. Deposition in the lung regions of an adult man calculated with the HPLD model (Table 2) compared to lung deposition data published by the ICRP, Annexe F (1994). Data are for a polydisperse aerosol with a mean particle diameter of 100 nm, a *GSD* of 1.5, a particle density of 3 g cm^{-3} and a shape factor of 1.5.

	Breathing path	***Q*** [m^3 h^{-1}]	***ET*** *[-]*	***TB*** *[-]*	***AL*** *[-]*	***TL*** *[-]*	**Annexe F page**
Figure 3A, HPLD, d_p = 100 nm	Nose	0.54	0.032	0.069	0.24	0.34	
ICRP, Annexe F, d_p = 100 nm	Nose	0.54	0.052	0.077	0.22	0.35	422
	Nose	0.45	0.052	0.082	0.20	0.33	418
	Nose	1.2	0.064	0.055	0.21	0.33	416
	Mouth	1.2	0.036	0.066	0.21	0.30	416
	Nose	1.5	0.066	0.051	0.21	0.32	426
	Nose	1.7	0.061	0.048	0.20	0.31	417
	Mouth	1.7	0.033	0.049	0.21	0.29	417
	Mouth	3.0	0.044	0.040	0.20	0.28	430